JAERI-M
87-081

DEVELOPMENT OF REALISTIC CHEST PHANTOM FOR CALIBRATION OF IN-VIVO PLUTONIUM COUNTING FACILITIES

June 1987

Takashi SHIROTANI

日 本 原 子 力 研 究 所
Japan Atomic Energy Research Institute

JAERI-Mレポートは，日本原子力研究所が不定期に公刊している研究報告書です。
入手の問合わせは，日本原子力研究所技術情報部情報資料課（〒319-11茨城県那珂郡東海村）あて，お申しこしください。なお，このほかに財団法人原子力弘済会資料センター（〒319-11 茨城県那珂郡東海村日本原子力研究所内）で複写による実費頒布をおこなっております。

JAERI-M reports are issued irregularly.
Inquiries about availability of the reports should be addressed to Information Division Department of Technical Information, Japan Atomic Energy Research Institute, Tokai-mura, Naka-gun, Ibaraki-ken 319-11, Japan.

編集兼発行　日本原子力研究所
印　　刷　いばらき印刷㈱

JAERI-M 87-081

Development of Realistic Chest Phantom for Calibration of in-vivo Plutonium Counting Facilities

Takashi SHIROTANI

Department of Health Physics
Tokai Research Establishment
Japan Atomic Energy Research Institute
Tokai-mura, Naka-gun, Ibaraki-ken

(Received May 11, 1987)

We have developed realistic chest phantom with removable model organs. The phantom is a torso and is terminated just above the femoral region. Tissue equivalent materials used in the phantom have been made of polyurethane with different amounts of ester of phosphoric acid, in order to simulate human soft tissues such as muscle, muscle-adipose mixtures and cartilage. Lung simulant has been made of foamed polyurethane. Capsulized small sources can be inserted into the holes, drilled in each sliced section of the model organ.

Counting efficiencies, obtained with a pair of 12 cm diameter phoswich detectors set above the phantom chest, are 0.195 cpm/nCi for Pu-239 and 44.07 cpm/nCi for Am-241, respectively. The results agree well with efficiencies obtained with IAEA-Phantom. We conclude that the phantom can be used as a standard phantom for the calibration of Pu chest counting equipment.

Keywords; Plutonium, Lung, Chest Wall, Counting Efficiency, Phantom, Calibration, Tissue Equivalent Material

JAERI－M 87－081

プルトニウム肺モニタ校正用精密ファントムの開発

日本原子力研究所東海研究所保健物理部
城谷　孝

（1987年5月11日受理）

肺に沈着したPu量を正確に測定するためには，検出器を人体ファントムを用いて校正しておかねばならない。PuはLX線のエネルギーが約17 keVと低いため，ファントム材は人体軟組織と同じ放射線特性をもたねばならない。原研では，6年ほど前からファントム素材の開発を行ない，筋肉，脂肪，軟骨などの素材を製作してきた。また，これらの素材を用い精密ファントムを開発した。ファントム素材は，ポリウレタンに少量のリン酸エステルを添加したもので，添加量を変えることによりさまざまな組織等価材を作製した。これらの材質の減弱係数は人体軟組織と一致している。この素材を用いたファントムは，計数効率，X線CT検査およびIAEAファントムとの比較試験などから，その特性が極めて良好であることを示した。

東海研究所：〒319－11　茨城県那珂郡東海村白方字白根2－4

CONTENT

目　　次

1. Introduction

There is a great need for a realistic human phantom*, in order to calibrate detector systems used for detection and quantification of Pu-239 and other actinides deposited in human lungs. In 1977, a new method for the formulation of tissue equivalent materials, called the "Basic Data Method", was published by White[1]. This method is very useful for manufacturing phantom materials for photons, in comparison with the existing methods such as the "Elemental Equivalence Method" and "Effective Atomic Number Method".

In 1978, Griffith *et al.*[2] presented the study of realistic human torso phantom in IAEA-Symposium. This phantom has been constructed of polyurethane with different concentrations of calcium carbonate, which simulate well the linear photon attenuation properties of human tissues at the low energy region such as the L-series radiations from Pu-239 (13.6, 17.2, 20.2 keV). This torso phantom has been adopted by IAEA as a standard phantom for the calibration of Pu chest counting equipment.

We have, since 1979, developed a realistic chest phantom having nearly the average physique of Japanese, which contains a human rib cage and removable model organs. Tissue equivalent materials developed for this purpose have been made of polyurethane with different amounts of the ester of phosphoric acid, in order to simulate various human soft tissues such as muscle, muscle-adipose mixtures and cartilage. In addition, a foamed polyurethane has been used as a lung simulant.

We made two torso phantoms**: The first phantom in 1983 was made for the purpose of obtaining basic data for realization of practical use. The second phantom, designed for the practical calibration, was completed in 1984, in which several improvements were made on the basis of the data obtained from the first phantom. We have called the second phantom "JAERI-phantom".

This paper describes the developed tissue equivalent materials (SZ-series materials), the construction of JAERI-phantom and its characteristics. In Appendix, moreover, the comparison of JAERI-phantom with IAEA-phantom is briefly described.

---

* In Ref.(9) are reviewed various tissue equivalent materials, which have been developed up to now, for realistic phantom.

** These phantoms were presented at 19th, 20th and 21th annual meetings of the Japan Health Physics Society.

2. Phantom Materials

Tissue equivalent materials, used as phantom materials, must have the same photon attenuation properties as those of human soft tissues being simulated. This is of particular importance for such low energy photons as the LX-rays from Pu-239, absorbed strongly in human tissue.

The phantom material consists of a base material, which is an organic compound having elemental composition similar to that of human tissue, and an additive, which is an inorganic compound with higher atomic number, added to the base material to achieve the proper X-ray transmission. In general, the log-log plots of photoelectric attenuation coefficients against photon energies for atoms and various compounds form linear graphs over certain energy regions. Figure 1 illustrates that we can overlap the straight line, S, for phantom material on the line, H, for human tissue, by adding optimum amount of a suitable additive to the base material.

In order to select base materials, we examined, from several viewpoint, whether or not various kinds of plastics such as lucite, epoxy, polyethylene, polystyrene, polyester, polyurethane and others can be used as base materials of good substitutes for human soft tissues. The results of the examinations showed that polyurethane is better suited as a base material than the others for the following reasons:

(a) It is very easy to vary the elemental composition of the material, by mixing small amounts of additive into polyurethane

(b) Polyurethane is also very easy to form into irregular shapes and its product is not deformed, cracked and broken by a shock, and

(c) Foamed polyurethane, which has a density of 0.24 - 0.31 g/cm^3, can be used as a lung simulant, and it can be easily produced

We must, however, pay attention to the slight change of density of polyurethane, which arises from the difference in ambient conditions, such as temperature, moisture and etc., in the manufacturing process.

2.1 Base materials and additive

Polyurethane consists basically of two fluid components, A (polyisocyanate) and B (polyol). However, there are various kinds of polyurethane added other organic compounds, which have different physical

properties each other. We have selected three kinds of polyurethane with different elemental compositions as base materials of soft tissue simulants, and also adopted the ester of phosphoric acid, which is liquid, as an additive, because the compound mixes uniformly well with the components of polyurethane in comparison with the additive of powder like calcium carbonate.

Table 1(a) shows the densities and elemental compositions of the base materials; SZ-50, SZ-49 and L-1. In this Table are also given, for reference, calculated electron densities of SZ-50 and SZ-49. Table 1(b) shows the physical data of two kinds of additives (the data of calcium carbonate are shown for comparison). SZ-50 has been widely used as a base material for muscle, muscle-adipose mixture and cartilage. SZ-49 has been used only as a base material for soft tissues containing much adipose such as chest plates, which are used to adjust adipose/muscle ratio in the chest wall of phantom, because of its lower density. L-1, which is a foamed polyurethane, has been used as a lung simulant.

2.2 Optimum amount of additive

Various tissue equivalent materials (phantom materials) have been made by adding different quantities of the additive to the base material. The optimum amount of the additive in the base material was theoretically calculated in such a way as the linear attenuation coefficient of the material becomes equal to that of the corresponding human tissue at one energy for one interaction of interest, as follows:

The relation among mass attenuation coefficients of phantom material, base material and additive is given by

$$\mu_p = b\,\mu_b + a\,\mu_a \qquad (1)$$

where μ_p, μ_b and μ_a are mass attenuation coefficients of phantom material, base material and additive, respectively, and b, a are proportions by weight, but

$$b + a = 1. \qquad (2)$$

In addition, the linear attenuation coefficient of the phantom

material must be equal to that of the corresponding human tissue;

$$\mu_p \, d_p - \mu_h \, d_h = 0 \qquad (3)$$

where μ_h is a mass attenuation coefficient of human tissue and d_h and d_p are the densities of human tissue and the phantom material, but

$$d_p = b \, d_b + a \, d_a \, . \qquad (4)$$

Using Eqs.(1) to (4), we can easily derive an optimum amount of additive, a, as follows;

$$a = \frac{1}{2\mu d} \left[\{ (\mu d_b + \mu_b d)^2 - 4\mu d(\mu_b d_b - \mu_h d_h) \}^{\frac{1}{2}} - (\mu d_b + \mu_b d) \right] \qquad (5)$$

where $\mu = \mu_a - \mu_b$ and $d = d_a - d_b$.

It is generally said that Compton scattering is relatively unimportant process of attenuation, because the cross sections for Compton scattering are smaller than those for photoelectric absorption in the low energy region such as Pu LX-rays. As shown in Fig. 2, the ratio of $\mu(P,C)$ to $\mu(C)$ for total soft tissue (see Table 108 in Ref.(4)) is about 0.17 at 16.6 keV, and this value appears to be not so small. However, Compton scattering cross section is less dependent on small amounts of the additive in the base material, because Compton scattering relates to electron density. Actually, the differences in the calculated electron densities between phantom materials and corresponding human soft tissues are very small, as shown in Table 2. In addition, the apparent effect of inaccuracy in Compton cross section of material may become smaller, because part of scattered photons escaped from the phantom chest are detected by using a detector with uncollimated large area window. Thus, the slight discrepancy can be tolerated than in the case of photoelectric absorption.

We also can neglect coherent scattering, because the scattering may be assumed not to result in any net loss.

2.3 Attenuation coefficients of phantom materials

Table 2 shows some examples of phantom materials; names, measured densities and calculated optimum amounts of additive. For reference, calculated electron densities and effective atomic numbers also are shown. SZ-208 and SZ-139 are muscle simulants, and SZ-208 is an improved material of SZ-139 which was used in the first phantom. SZ-220 and SZ-207 correspond to (muscle + 10% adipose) and (muscle + 23% adipose), respectively. SZ-207 is a substitute of the total soft tissue. SZ-160 is a cartilage simulant, in which SZ-50U* was used as a base material, and also SZ-209 is a cartilage simulant used SZ-50.

For each of the phantom materials and human tissues, we calculated theoretically partial mass and linear attenuation coefficients for photoelectric interactions, coherent and incoherent scattering in the energy range from 8 keV to 1 MeV. In this calculation were used McMaster's "X-ray Cross Section Tables"[3] and Table 108 "Elemental Content of Organs and Tissues of Reference Man" in ICRP Publication 23[4]. Table 3 shows the calculated linear attenuation coefficients of the materials, human tissues and water for the energy region of Pu LX-ray. For comparison, the coefficients of Griffith-muscle (polyurethane + 4.3% $CaCO_3$)[6] and RANDO-muscle[5),6)] also are listed in this Table. The accuracy of the calculated coefficients depends principally on the uncertainty in the values of the cross sections of elements and inaccuracy of the elemental compositions in the organs and tissues of reference man.

Log-log plots of the calculated photoelectric attenuation coefficients of the materials against energy form linear graphs over certain energy range. Figures 3 to 7 show the linear relationship for the SZ-series materials and corresponding human tissues. The degree of discrepancy between the both lines at a given energy can be numerically expressed by R-value defined as

$$R = \mu_p/\mu_h \qquad (5)$$

where μ_p and μ_h are linear attenuation coefficients of a given material and corresponding human tissue, respectively. For example, calculated

---

* See marginal note of Table 1(a).

R-value of SZ-208 are 1.0034 at 17.2 keV and 0.9898 at 60 keV for $\mu(P)$, respectively. The R-value depends on the slope of the straight line, which changes by the elemental composition of material, especially additive.

We have measured the photon transmissions of the materials, using 16.6 keV X-rays from Nb-93m and 60 keV gamma rays from Am-241. Figures 8 and 9 show observed transmission curves. In Fig. 9, for comparison, also are shown transmission curves of water and human tissues, obtained from calculations. The Figures show that the observed curves agree well with the calculated.

The transmission curve of L-1 depends strongly on the state of foaming of polyurethane. Therefore, we have selected better quality with density from 0.25 to 0.32 g/cm^3 out of the products carefully foamed, because it has not been so easy to control strictly the degree of foaming. We have usually used L-1 added small amount of the ester of phosphoric acid for adjusting the attenuation coefficient.

The discrepancy between the observed transmission curve of the substitute and the calculated curve of corresponding human tissue can be also estimated by using Eq.(5), but μ_p takes a value computed from the observed curve. The quality of produced phantom material can be judged from the estimated R-value, and if necessary, the amount of additive is adjusted.

Figure 10 also shows the transmission curves obtained from SZ-series, beef (lean muscle), fat, water, RANDO-muscle and lung. The data of (polyurethane + 4.3% adipose) in Fig. 10 are reprinted from Griffith's paper[2]. The measurements were made using NaI(Tl)-detector without collimator for comparison with Griffith's data. The curve from beef may not be completely accurate, because of the evapolation of water in beef and the degeneration of beef under measurements. The two dot-lines from RANDO-lung were obtained from different parts of the sliced lung sections.

These observed results show that there are not problems in the attenuation properties of SZ-series materials, but RANDO-muscle is not suitable for low energy photons such as Pu LX-rays.

3. Construction of Chest Phantom and Its Characteristics

3.1 Phantom construction

A chest phantom containing human rib cage and removable model organs has been constructed. This phantom constructed with SZ-series materials is a torso and is terminated just above the femoral region. Figure 11(a) shows the completed phantom with chest plate in place, and Fig. 11(b) shows the phantom chest with chest plate and torso cover removed showing organs. Table 4 shows the body size, the volume of removable model organs and the names of substitutes used in each part of the phantom. The physique of phantom, in general, is decided by the size of an available human rib cage. For that reason, the body size of the phantom in this Table became smaller than the average size of Japanese adult males*. The used human rib cage were cleaned, the marrow was removed and the lost marrow was replaced with SZ-50.

Capsulized point sources can be inserted into the holes, which were drilled in the specified positions of each part of the removable model organ sliced at regular intervals, as seen in RANDO-phantom (Alderson Research Laboratories). The size of the capsule is 4 mm in diameter × 20 mm in length and is made of polypropylene tubing with wall thickness of 0.1 mm. The trachea is not removable but it is possible to insert source capsules into the organ.

Figure 12 illustrates the chest plate overlaid on the phantom chest. The chest plates are used in order to simulate the chest wall attenuation of the wide range of adipose/muscle ratio seen in adult males. The thickness of the chest plate is 0.8 cm, and the total thickness of the frontal chest wall is 2.3 cm, as shown in Fig. 12. The total thickness is equal to the average chest wall thickness, which was obtained from the ultrasonic measurements of chest wall thickness made on 70 male subjects[7]. The adipose/muscle ratios in the Table on Fig. 12 are not the ratios of each chest plate material itself, but indicates the ratio of the total chest wall (chest plate + torso cover). Chest plates with different thickness will be produced in the near future.

---

* Average sizes for height, weight and chest circumference are nearly 1.69 m, 63.5 kg and 0.91 m, respectively.

3.2 Examination of phantom using X-ray CT-Scanner

We examined the quality of the phantom using X-ray Computed Tomographic Scanner in Tokyo Daini Hospital. Figure 13 shows an example out of tomograms obtained from the cross sectional scans of the lung region. We measured CT-values* of different positions (i.e. different materials) in the phantom, and derived linear attenuation coefficients from the CT-values. In this calculations, the linear attenuation coefficient of water at 60 keV, 0.1904, was used, because the X-ray effective energy of the scanner was approximately 60 keV (working voltage: 120 kV). The results are shown in Table 5. For comparison, in column (iii) of the Table are given the linear attenuation coefficients calculated from the elemental composition of each material. The agreement between the observed and calculated attenuation coefficients suggests that the phantom will provide an accurate measurement of internal attenuation of low energy photons.

3.3 Counting efficiencies

The counting efficiencies of the Pu chest counting detector**, installed in the iron room***, were determined from measurements of the phantom having point sources within the lungs under the conditions of standard geometry****. Average woman RANDO-phantom also was measured

---

* CT-value is defined as follows; CT-value = $1000(\mu_p - \mu_w)/\mu_w$, where μ_p and μ_w denote linear attenuation coefficients of the phantom material in question and water, respectively. The relation between measured CT-value, H_m, and calculated true CT-value, H_t, is given by $H_t = 1000(H_m - H_w)/(H_w - H_a)$, where H_w and H_a are experimental CT-values for water and air, called *calibration factor*, respectively.

** The most common arrangement of two 12 cm diameter phoswich detectors (3 mm thick NaI/3 cm thick CsI, 0.3 mm thick Be-window).

*** The inner size of the iron room is height 2.0 m, width 1.0 m and length 2.0 m. The thickness of iron wall is 20 cm and inside of the room is lined with lead 0.5 mm thick.

**** The detectors were set above the chest of the supine phantom with the edge of each detector window above the clavicle and minimum clearance of 1 cm between the window and the surface of the chest.

under the same conditions in order to compare with the data obtained from JAERI-phantom.

The total activities of Pu and Am-sources inserted in the lungs of JAERI-phantom and RANDO-phantom are listed in Table 6. The elemental composition of the used Pu-source is shown in the marginal note of Table 6. The numbers of point source capsules in the right and left lungs of JAERI-phantom are 77 and 70, respectively, and these numbers in RANDO-phantom are 74 in right and 63 in left.

Table 7 shows the counting efficiencies for Pu-239 and Am-241, obtained from RANDO-phantom and JAERI-phantom with and without the chest plate under the condition of standard geometry. The counting efficiency of JAERI-phantom with the chest plate (SZ-2120) is 0.093 cpm/nCi for the Pu-source. We belive that this value has high reliability in comparison with the counting efficiency predicted from the photon attenuation in muscle and the results obtained from measurements of IAEA-phantom. (See Appendix for the measurements of IAEA-phantom).

We also examined the variation of counting efficiency resulting from the differences in the detector-body-geometry, as shown in Figs. 14(A), (B) and (C). Figure 15 shows the variation of counting efficiency of the detector shifted from the standard position to the abdomen along the body axis as shown in Figs. 14(A) and (B). The shape of the curves from RANDO-phantom differs from others, suggesting that there may be some problems in the anatomical structure of RANDO-phantom and the source distribution in the lungs. Recently, Sekiguchi *et al.*[8] have shown, by means of "Monte Carlo Simulation" of Pu chest counting, that the distribution pattern of photons emitted through the frontal chest of RANDO-phantom with uniformly distributed Pu-239 source in the lungs is strongly localized at the neighborhood of low lobes (see Fig. 4 in Ref.(7)). Their results explain well the shape of the curves from RANDO-phantom shown in Fig. 15. They have also pointed out that the anatomical structure of RANDO-phantom is not so good.

Figure 16 shows the variation of counting efficiency of the detector moved right and left from the standard position, as seen in Fig. 14(C). It is an expected result that the counting efficiency of detector shifted to the right is slightly larger than that to the left. Figure 17 shows the decrease in the counting efficiency of the detector moved externally along the normal direction from the chest surface at the standard position.

Furthermore, we investigated the rate of increase in background counts in LX-ray and gamma-ray energy regions, which arises from Am-241 deposited in the liver. The Am sources inserted in the liver of JAERI- and RANDO-phantoms are 20.77 and 22.78 nCi, respectively. The observed results are shown in Table 8. In the case of the Pu-source, the significant increase in background counts was not observed. However, in actual chest counting for a person inhaled pltonium dust, we should pay attention to the slight increase of background arising from the dust transfered to the liver, because the dust contains generally small quantity of americium which is the daughter of Pu-241.

4. Conclusion

The X-ray attenuation characteristics of SZ-series materials, obtained from the experiments, agree well with those of corresponding human tissues, calculated from their elemental compositions, and also the counting efficiencies obtained from the calibration experiments are reasonable values. The tomograms obtained with X-ray CT-scanner show that there are no problems for the phantom construction and its materials. The experimental results have proved that the phantom constructed with SZ-series materials can be used in the calibration of Pu lung counting equipment and in other experiments, as a standard phantom.

In manufacturing process of phantom materials, one of the most important things is to control precisely each density of the materials. There still remain, moreover, some important problems to be solved, as described below:

(1) Establishment of high quality foamed polyurethane manufacturing process for lung simulant,

(2) Development of an artificial rib cage; it is necessary to manufacture a phantom of the same body size with the average physique of Japanese adult males. For this purpose, an artificial bone must be developed, and

(3) Improvement in the source capsule; it is very useful to make a smaller size capsule, using the same material with organ substitutes.

We have already started to develop an artificial bone. A standard size chest phantom with artificial rib cage will be completed before long. The improvements on (1) and (2) described above also are under investigation now.

Acknowledgments

The author would like to thank Mr. H. Sugimoto and Mr. T. Takayama of Kyoto Kagaku Hyohon Co. Ltd., for manufacturing both SZ-series materials and JAERI-phantom. The author is also exceedingly grateful to Mr. Y. Ohi for the measurements of the phantoms, to Mr. T. Hattori for the preparation of Pu and Am sources, and to Mr. S. Suga for the revision of manuscript.

4. Conclusion

The X-ray attenuation characteristics of SZ-series materials, obtained from the experiments, agree well with those of corresponding human tissues, calculated from their elemental compositions, and also the counting efficiencies obtained from the calibration experiments are reasonable values. The tomograms obtained with X-ray CT-scanner show that there are no problems for the phantom construction and its materials. The experimental results have proved that the phantom constructed with SZ-series materials can be used in the calibration of Pu lung counting equipment and in other experiments, as a standard phantom.

In manufacturing process of phantom materials, one of the most important things is to control precisely each density of the materials. There still remain, moreover, some important problems to be solved, as described below:

(1) Establishment of high quality foamed polyurethane manufacturing process for lung simulant,

(2) Development of an artificial rib cage; it is necessary to manufacture a phantom of the same body size with the average physique of Japanese adult males. For this purpose, an artificial bone must be developed, and

(3) Improvement in the source capsule; it is very useful to make a smaller size capsule, using the same material with organ substitutes.

We have already started to develop an artificial bone. A standard size chest phantom with artificial rib cage will be completed before long. The improvements on (1) and (2) described above also are under investigation now.

Acknowledgments

The author would like to thank Mr. H. Sugimoto and Mr. T. Takayama of Kyoto Kagaku Hyohon Co. Ltd., for manufacturing both SZ-series materials and JAERI-phantom. The author is also exceedingly grateful to Mr. Y. Ohi for the measurements of the phantoms, to Mr. T. Hattori for the preparation of Pu and Am sources, and to Mr. S. Suga for the revision of manuscript.

REFERENCES

(1) D.R. White : "The Formulation of Tissue Substitute Materials using Basic Interaction Data", Phys. Med. Biol., Vol.22, 889 (1977).

(2) R.V. Griffith, P.N. Dean, A.L. Anderson and J.C. Fisher : "Fabrication of a Tissue-equivalent Torso Phantom for Intercalibration of In-Vivo Transuranic-Nuclide Counting Facilities", UCRL-80343, 1978.

(3) W.H. McMaster, N. Kerr Del Grande, J.H. Mallett and J.H. Hubbell : "Compilation of X-Ray Cross Sections", UCRL-50174R, 1969.

(4) ICRP Publication 23 : "Report of the Task Group on Reference Man", Pergamon Press, New York, 1975.

(5) S.W. Alderson, L.H. Lanzl, M. Rollins and J. Spira : "An Instrumented Phantom System for Analog Computation of Treatment Plants", American J. of Roentgenology, Vol.87, 185 (1962).

(6) D. Newton and D.R. White : "Attenuation of 13－20 keV Photons in Tissue Substitutes and Their Validity for Calibration Purposes in the Assessment of Plutonium in Lungs", Health Phys., Vol.35, 699 (1978).

(7) T. Shirotani and Y. Ohi : "An Optimum Form of Regression Equation for Estimating Chest Wall Thickness in Pu Lung Counting", Health Phys., Vol.50, 860 (1986).

(8) M. Sekiguchi, M. Endo, T.A. Iinuma and O. Matsuoka : "Monte Carlo Simulation of Pu Lung Counting Using X-ray CT Image Data of Commercially Available Anthropomorphic Phantom", HOKEN BUTSURI, Vol.21, 185 (1986) (in Japanese).

(9) T. Shirotani : "Progress of Tissue Equivalent Materials", NIHON-GENSHIRYOKU-GAKKAISHI, Vol.28, 25 (1986) (in Japanese).

[APPENDIX]

Comparison of JAERI-Phantom with IAEA-Phantom

In 1985, a rare oppotunity for borrowing IAEA-phantom* was given us by participating in the interlaboratory comparison of calibration techniques for measuring lung contamination of Pu and other actinides in vivo by means of realistic chest phantom, supported by IAEA Nuclear Safety Division**. We calibrated our Pu chest counting equipment*** with IAEA-phantom, and also examined the differences between JAERI-phantom and IAEA-phantom. The results are briefly itemized bellow:

(1) Table A-1 shows the body parameters of IAEA-phantom and JAERI-phantom, and the used phantom materials. IAEA-phantom is considerably bigger than JAERI-phantom. Figure A-1 illustrates the front views of the both phantoms removed torso cover, in order to show the differences in the shape and size of organs. The IAEA-phantom materials, C1-121, C-130 and C2-162 are muscle simulants. A-113 and B-119 are muscle-adipose mixture simulants corresponding to (87% + 13% adipose) and (50% muscle + 50% adipose), respectively.

(2) Table A-2 shows the linear attenuation coefficients of the IAEA-phantom materials, which were calculated from the elemental composition of each material, using measured densities and McMaster's X-ray cross section table, by the present author. In Table A-2 are, for comparison, shown again the coefficients of SZ-series materials.

(3) Figure A-2 shows the transmission curves obtained from IAEA-phantom materials, together with the curves of SZ-series. The observed curves for C1-121, C-130 and C2-162 agree well with the calculated results and with the curve of SZ-208 within a permissible error. The observed curves, however, for A-113 and B-119

---

* IAEA-phantom is the same with the realistic chest phantom developed by Griffith *et al.*[2].

** Formal name of the meeting is "Use of Realistic Chest Phantom for the Calibration of Counting Facilities for the Assessment of Plutonium and other Actinides Deposited in Lung".

*** See the footnotes of section 3.3 in the text.

differ from the calculated, as shown in Fig. A-2. This disagreement indicates that A-113 corresponds to (25% muscle + 75% adipose) and B-119 to (60% muscle + 40% adipose), suggesting that there may be some problems for the accuracy of the amount of additive ($CaCO_3$) in the base material (the measured densities of A-113 and B-119 were about 1.055 and 1.080 g/cm^3, respectively).

(4) Table A-3 shows counting efficiencies obtained with IAEA-phantom without chest plate under the condition of the standard geometry. The chest wall (torso cover) thickness is 1.54 cm. The slight discrepancies in the counting efficiencies between IAEA-phantom and JAERI-phantom may result from the differences in isotopic composition of Pu-source, chest wall thickness, lung size and shape shown in Fig. A-1, and source distribution pattern within lungs.

(5) Figure A-3 shows the variations of counting efficiency of the detector shifted from the standard position to the abdomen along the body axis. The decrease in the efficiency of IAEA-phantom is extremely large. This may arise from the differences in the anatomical shape and size of the lungs.

(6) Figure A-4 shows the variation of the counting efficiencies of the detector shifted directionally right and left from the standard position. The efficiency at the right side is extreamly high as compaired with that at the left, in the case of IAEA-phantom, for Pu-source.

We conclude, judging from these experimental results described above, that (1) there are no problems about the photon attenuation properties of SZ-series materials, (2) the differences in characteristics between JAERI-phantom and IAEA-phantom, as seen in Figs. A-3 and A-4, arise from the differences in the shape and size of the lungs between the both phantoms as shown in Fig. A-1, and (3) consequently, laboratories in each country should have a standard realistic chest phantom with average body size of people in his own country. For the spread of realistic phantom, however, it is necessary to establish an international quality standard for tissue equivalent materials used in the phantom.

Table 1 Base materials and additives

a) Base materials		SZ-50 (SZ-50U**)	SZ-49	L-1***
Density* (g/cm^3)		1.052 (1.074**)	0.990	0.280
Elemental composition (w_t%)	H	8.49	9.18	6.20
	C	72.26	71.99	60.05
	N	4.49	2.46	5.60
	O	14.76	16.37	28.15
Electron density (n/cm^3)		3.44×10^{23}	3.27×10^{23}	

* Measured value, ** Hardness type of SZ-50,
*** Foamed polyurethane

b) Additives	Ester of phospharic acid $(C_2H_4ClO)_3PO$ (liquid)	Calcium carbonate $CaCO_3$ (powder)
Density* (g/cm^3)	1.43	2.73
Photoelectric mass att. coeffi.** (cm^2/g)		
17.2 keV	5.442	8.139
60.0 keV	0.109	0.183

* Measured value, ** Calculated value

Table 2 Examples of tissue equivalent materials

Materials	SZ-208	SZ-207	SZ-220	SZ-139	SZ-160 (SZ-209)
Corresponding human tissue	muscle	total soft tissue *	muscle + 10% adipose	muscle	cartilage
Base material	SZ-50	SZ-50	SZ-50	SZ-50U	SZ-50U (SZ-50)
Amounts of additive (wt%)	8.48	6.22	7.35	8.20	9.00 (9.30)
Density** (g/cm^3)	1.075	1.067	1.069	1.116	1.117 (1.078)
Electron density (g/cm^3)	3.48×10^{23} (3.51×10^{23})***	3.46×10^{23} (3.32×10^{23})***	3.47×10^{23}	3.63×10^{23}	3.62×10^{23} (3.65×10^{23})*** (—)
Effective atomic number (Z_{eff})	7.27	7.01	7.14	7.24	7.33 (—)

* See Table 108 in ICRP Pub. 23, ** Measured values, *** Values for corresponding human tissues

Table 3 Calculated linear attenuation coefficients of the tissue equivalent materials and human tissues for Pu L-series radiations

μ (P) : attenuation coefficient for photoelectric interactions

μ (C) : attenuation coefficient for Compton scattering

	Linear attenuation coefficients (cm^{-1})					
	13.6 keV		17.2 keV		20.2 keV	
	μ (P)	μ (C)	μ (P)	μ (C)	μ (P)	μ (C)
SZ-50	0.876	0.172	0.403	0.180	0.237	0.187
SZ-208	1.823	0.173	0.873	0.182	0.528	0.189
SZ-207	1.571	0.171	0.748	0.180	0.450	0.186
SZ-220	1.690	0.173	0.808	0.182	0.487	0.188
SZ-139	1.861	0.180	0.891	0.189	0.538	0.196
SZ-160 (SZ-209)	1.954	0.180	0.937	0.189	0.567	0.196
(Polyurethane+4.3%$CaCO_3$)*	1.720	0.179	0.824	0.186	0.498	0.190
RANDO-muscle* 1)	1.500	0.166	0.700	0.173	0.423	0.175
2)	1.030	0.167	0.465	0.174	0.279	0.176
Human tissue: muscle	1.851	0.170	0.870	0.179	0.519	0.186
Human tissue: adipose	0.879	0.157	0.408	0.164	0.243	0.169
Human tissue: muscle + 10% adipose	1.744	0.169	0.819	0.178	0.489	0.184
Human tissue: muscle + 23% adipose	1.627	0.167	0.764	0.176	0.456	0.182
Human tissue: cartilage	1.961	0.179	0.921	0.188	0.549	0.195
Human tissue: lung	0.506	0.045	0.238	0.048	0.142	0.050
Human tissue: rib bone	7.760	0.192	3.833	0.204	2.367	0.212
Water	1.731	0.164	0.809	0.172	0.480	0.179

* See Table 2 in Ref. (6).

Table 4 Dimensions and materials of JAERI—phantom

Body parameters	Height	1.65 m
	Weight	56.3 kg
	Chest circumference	0.84 m*
	Chest width	0.283 m*
	Chest thickness	0.203 m*
Organ volumes	Lungs right	1765 cm3
	left	1614 cm3 (ρ=0.29g/cm^3)
	Kidnys right	158 g
	left	156 g
	Liver	1644 g
	Heart	903 g
Used substitutes	Trunk	SZ—220
	Lung	L—1
	Kidney	SZ—208
	Liver	SZ—208
	Cartilage	SZ—160
	Trachea	SZ—208
	Chest plate	SZ—2110
		and others

* Values for phantom with chest plate in place (see Fig. 11(a))

Table 5 Observed CT-values and linear attenuation coefficients of phantom materials, obtained from CT-scanner

(i) Observed CT-values
(ii) Linear attenuation coefficients derived from CT-values
(iii) Linear attenuation coefficients calculated from elemental composition of each substite

	(i)	(ii)	(iii)
Trunk (SZ-220)	54.3	0.201	0.199
Heart,Liver and Kidney (SZ-208)	61.3	0.208	0.201
Lung (L-1)	784	0.041	0.051
Cartilage (SZ-160)	78.8	0.205	0.209

Table 6 Radioactive sources inserted into the phantoms

	Activities in lungs (nCi)	
Nuclides	JAERI—Phantom	RANDO—Phantom
Pu—239*	1147.2	935.44
Am—241	200.76	91.79

* Elemental composition of the Pu-source (Wt%) :
Pu-239=99.121, Pu-240=0.868, Pu-241=0.00635, Pu-242=0.00496

Table 8 Increase of background counts resulting from Am-241 in the liver

	Increase of background counting rate(cpm/nCi)	
	LX-ray channel (13-24keV)	Gamma-ray channel (45-68keV)
Without chest plate*	0.95	8.28
With chest plate*	0.90	7.80

* SZ-2120 (see Fig.12)

Table 7 Counting efficiencies obtained from chest counting of JAERI—Phantom and RANDO—phantom under the condition of standard geometry

	Counting efficiencies (cpm/nCi)			
Nuclide in lungs	Pu-239		Am-241	
Energy band	LX—ray (13-24 keV)		γ—ray (45-68 keV)	
Chest plate	Without	With	Without	With
JAERI-phantom	0.195	0.093*	44.07	35.52*
RANDO-phantom**	0.228	—	42.49	—

* Obtained with SZ-2120 (See Fig. 12)
** Estimated chest wall thickness = 1.3 cm

Table A—1 Comparison of body and organ sizes between JAERI—phantom and IAEA—phantom

		Body and organ sizes	
		JAERI	IAEA
Body parameters	Height	1.65 m	1.77 m
	Weight	56.3 kg	75.0 kg
	Chest circumference	0.84 m*	1.01 m**
	Chest width	0.283 m*	0.335 m**
	Chest thickness	0.203 m*	0.240 m**
Organ volumes	Lungs right	1765 cm^3	2180 cm^3
	left	1614 cm^3 (ρ = 0.29 g/cm^3)	1689 cm^3 (ρ = 0.28 g/cm^3)
	Kidnys right	146.3 cm^3	150 cm^3
	left	144 cm^3	170 cm^3
	Liver	1522 cm^3	2050 cm^3
	Heart	836 cm^3	748 cm^3
	Spleen	—	171 cm^3
Used substitutes	Trank	SZ—220	C1—121
	Lung	L—1	F—113—11+ 504 R, L++
	Kidny	SZ—208	C2—162
	Liver	SZ—208	C2—162
	Cartilage	SZ—160	—
	Trachea	SZ—208	—
	Lymphnode	—	502L. S1, S2 +++
	Chest plate	SZ—2110 and others	A—113, B—119, C—130

* Values for phantom with chest plate in place (see Fig. 11(a))
** Values for phantom without chest plate
\+ Lung simulant labelled with Am-241, ++ Lung simulant labelled with Pu-239
+++ Lymphnode simulant labelled with Am-241

Table A—2 Linear attenuation coefficients of JAERI—phantom and IAEA—phantom materials for Pu L—series radiations, calculated from elemental composition of each material
(Measured densities were used in the calculations)
μ(P) : attenuation coefficient for Photoelectric interactions
μ(C) : attenuation coefficient for Compton interactions

		Linear attenuation coefficients (cm^{-1})					
		13.6 keV		17.2 keV		20.2 keV	
		μ(P)	μ(C)	μ(P)	μ(C)	μ(P)	μ(C)
IAEA-phantom materials	C—130	1.733	0.179	0.832	0.188	0.504	0.195
	B—119	1.378	0.177	0.638	0.186	0.382	0.193
	A—113	0.978	0.174	0.452	0.183	0.266	0.189
JAERI-phantom materials	SZ—50	0.876	0.172	0.403	0.180	0.237	0.187
	SZ—208	1.823	0.173	0.873	0.182	0.528	0.189
	SZ—207	1.571	0.171	0.748	0.180	0.450	0.186
	SZ—220	1.690	0.173	0.808	0.182	0.487	0.188

Table A—3 Counting efficiencies

	Counting efficiencies (cpm/nCi)	
Nuclide (energy band)	Pu—239 (13-24 keV)	Am—241 (45-68 keV)
JAERI—Phantom	0.195*	44.07
IAEA—Phantom	0.172**	40.70

* See marginal note of Table 6 for elemental composition of JAERI Pu source
** Elemental composition of IAEA Pu source: Pu-238=0.00706, Pu-239=99.986 Pu-240=0.006, Pu-241=0.00037, Pu-242=0.00034 (Wt%)

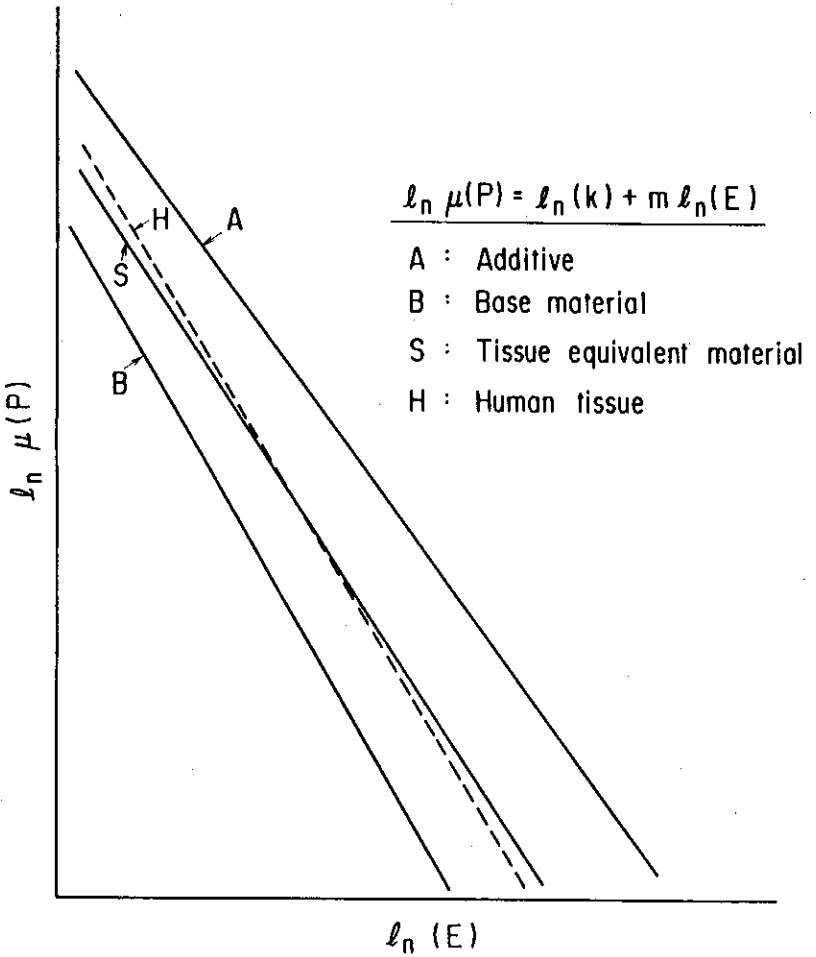

Fig.1 Relationship between ln(μ(P)) and ln(E) for base material, additive, tissue equivalent material and human tissue

μ(P): cross section for photoelectric interactions

E: energy, m, k: constants

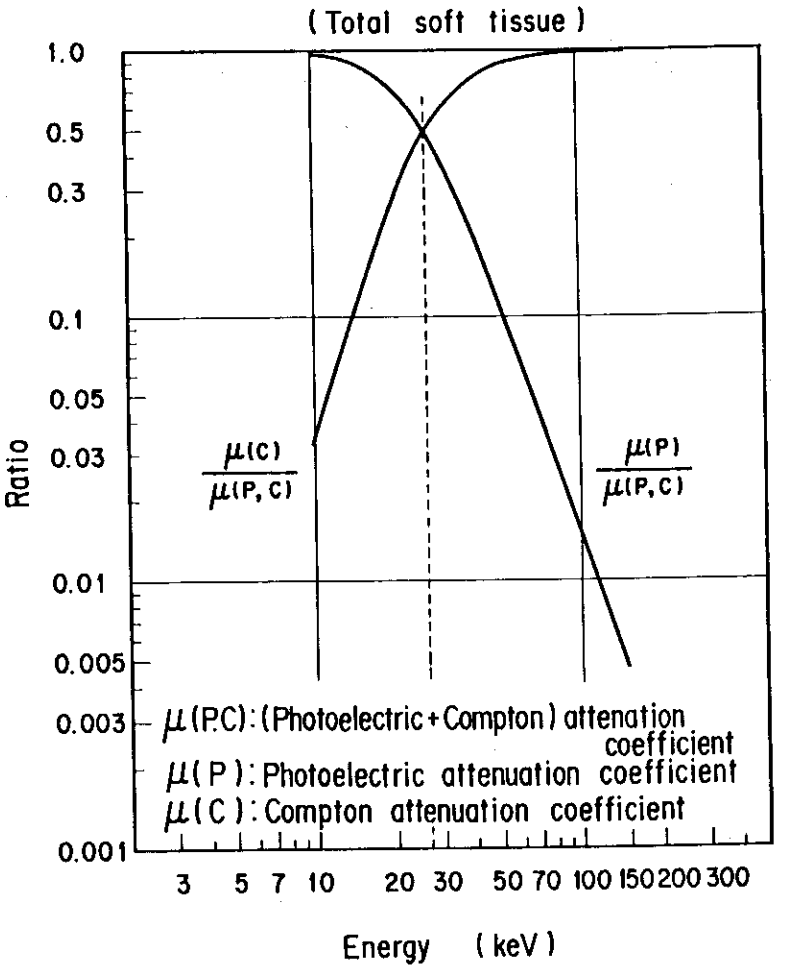

Fig.2 Graphs of μ(P)/μ(P,C) and μ(C)/μ(P,C) against ln(E)

μ(P): cross section for photoelectric interactions

μ(C): cross section for Compton interactions

μ(P,C) = μ(P) + μ(C), E: energy

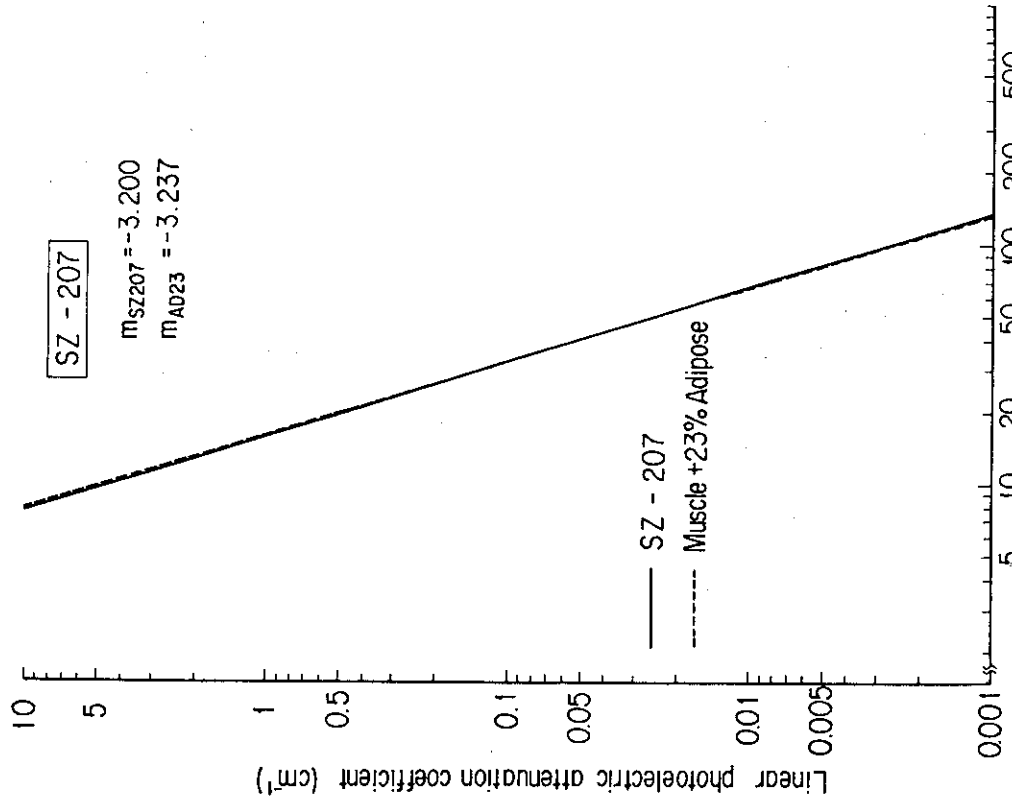

Fig.4 Graphs of ln(μ(P)) against ln(E) for SZ-207 and muscle+23%adipose

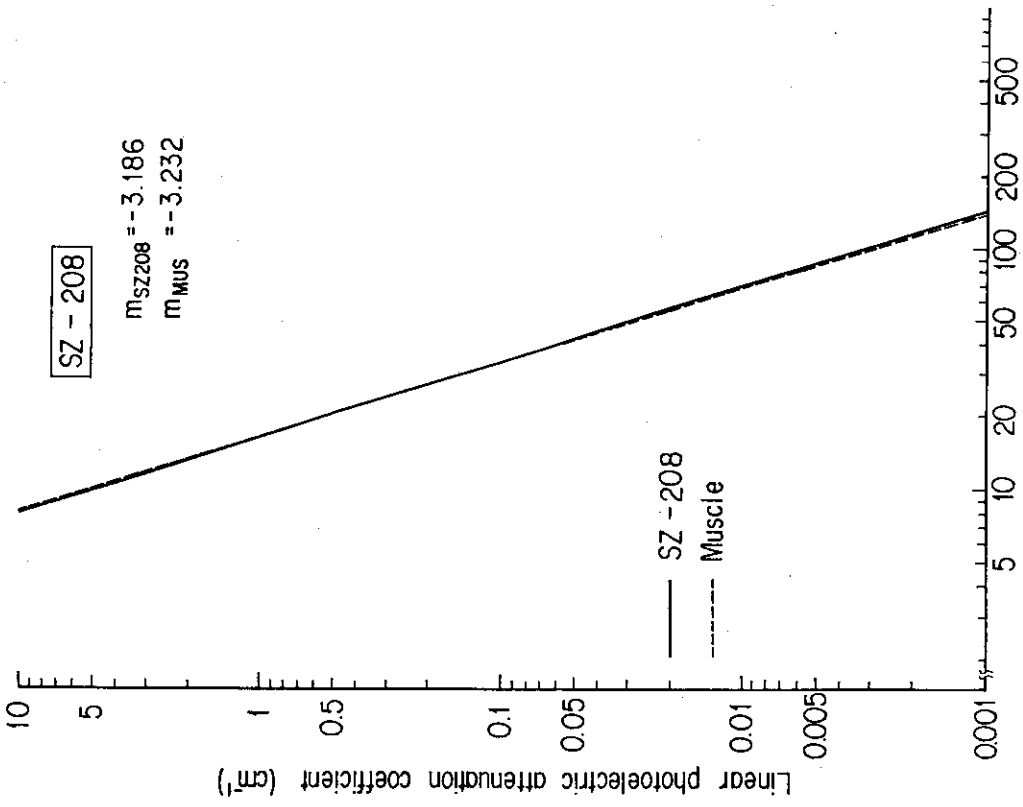

Fig.3 Graphs of ln(μ(P)) against ln(E) for SZ-208 and muscle

m: slope of curve from each material

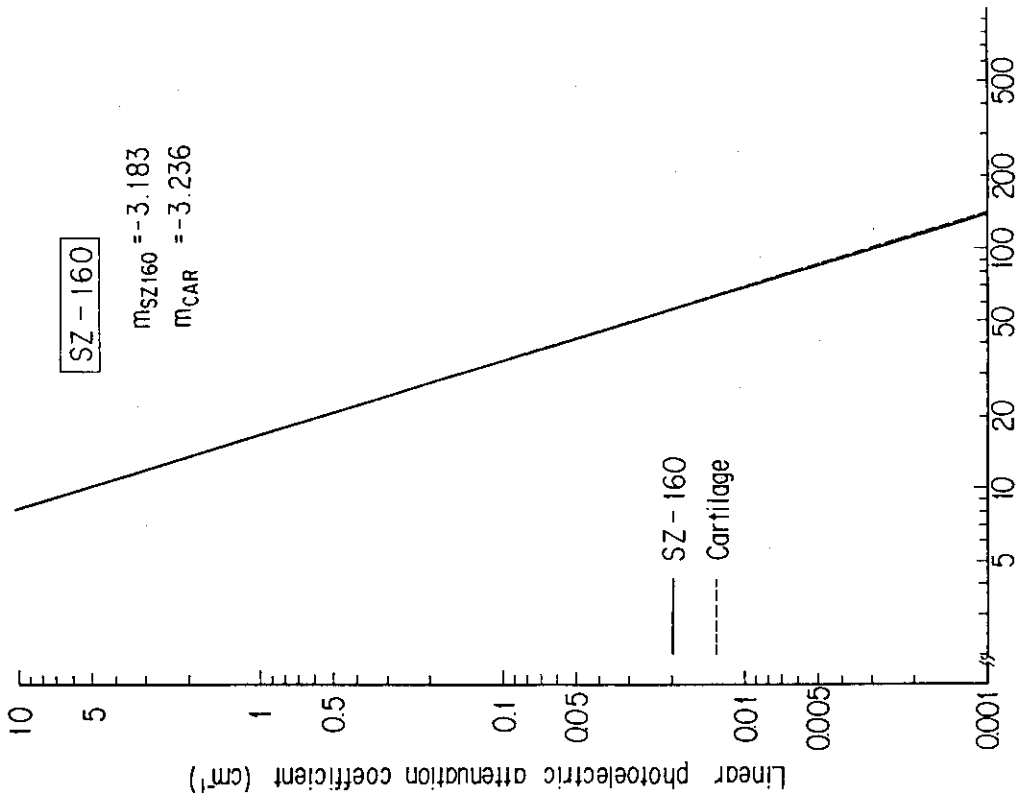

Fig.6 Graphs of ln(μ(P)) against ln(E) for SZ-160 and cartilage

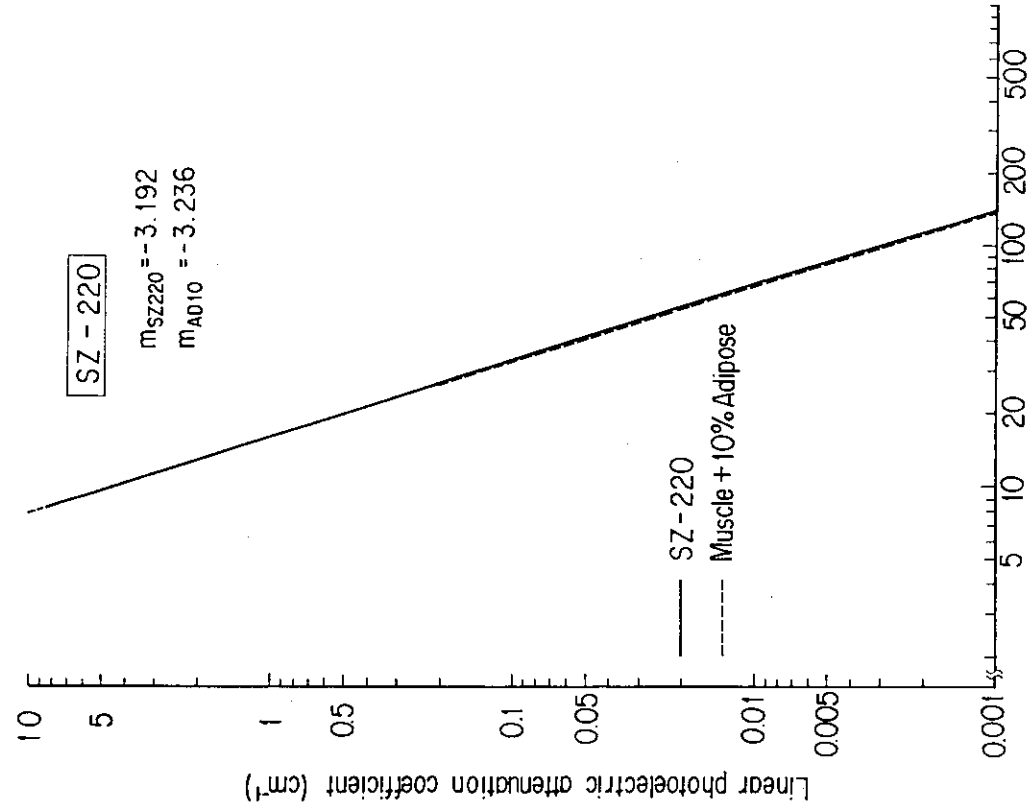

Fig.5 Graphs of ln(μ(P)) against ln(E) for SZ-220 and muscle+10%adipose

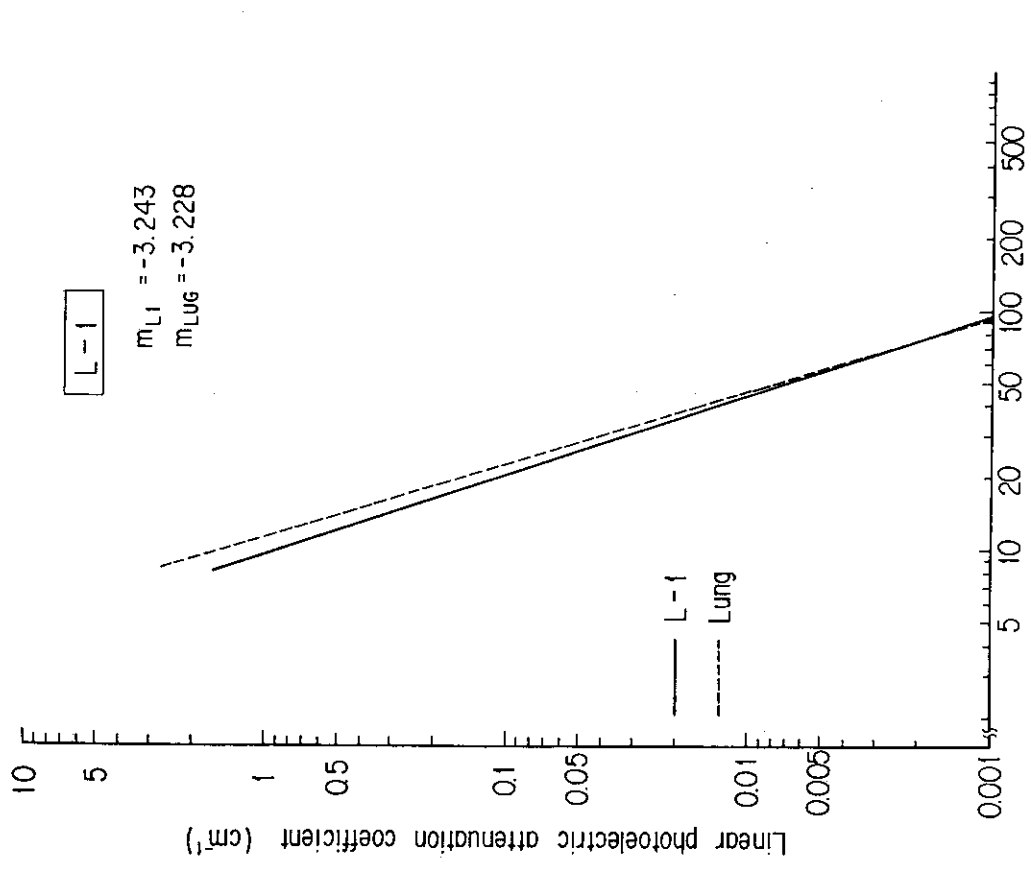

Fig.7 Graphs of ln(μ(P)) against ln(E) for L-1 and lung

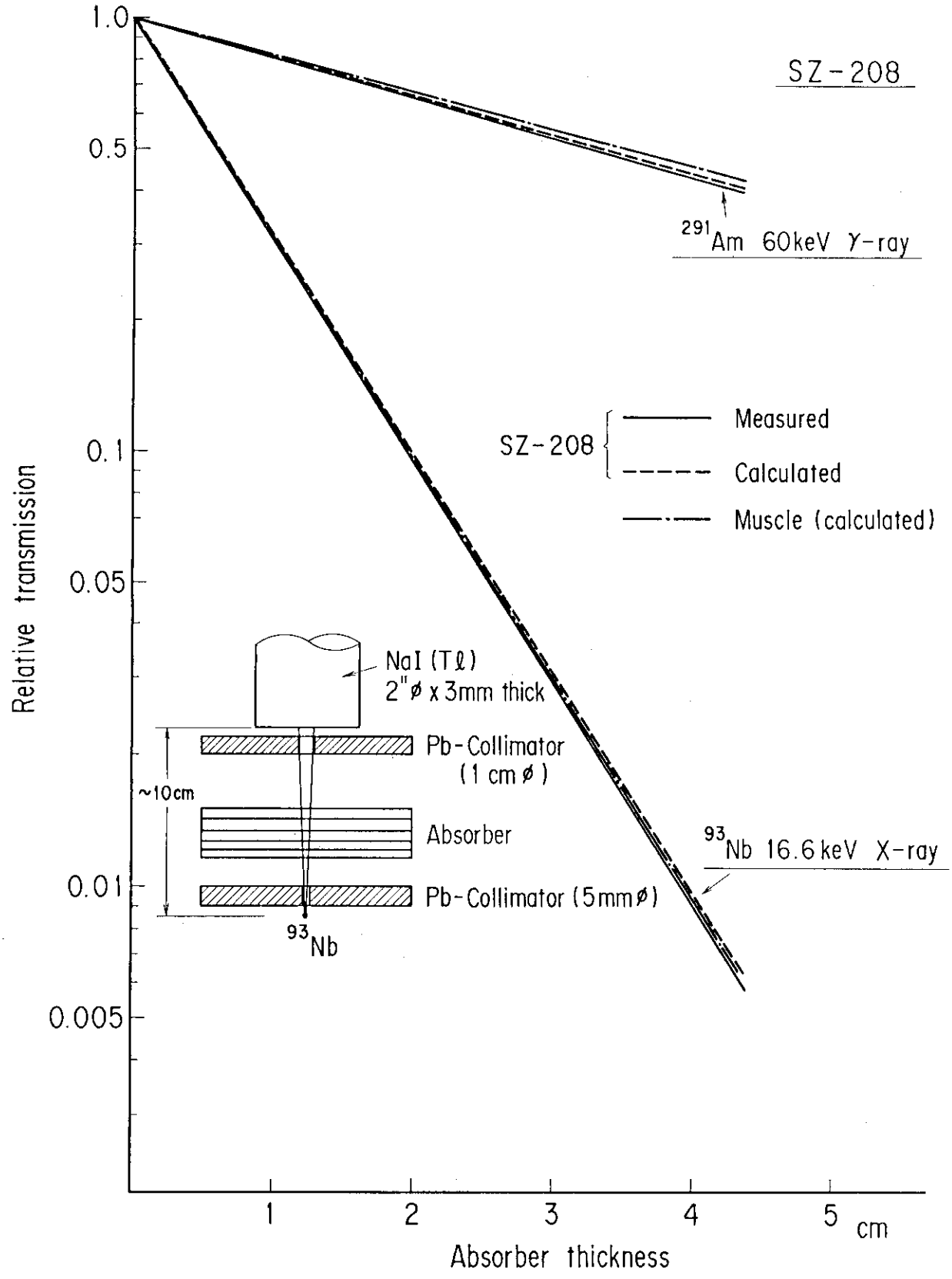

Fig.8 Relative X- and gamma-rays transmission through SZ-208 and muscle

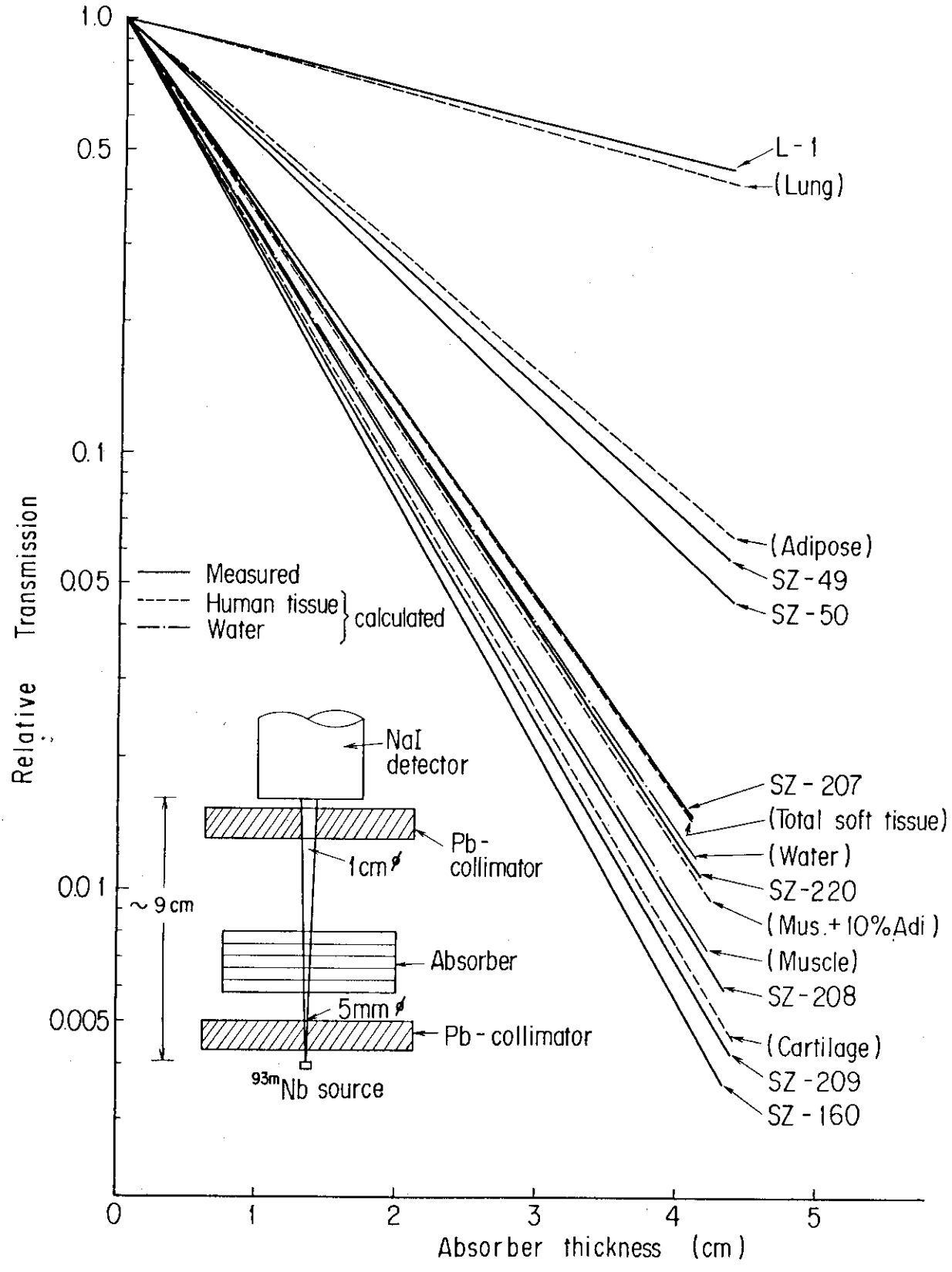

Fig.9 Relative X-ray transmission through SZ-series materials and corresponding human tissues

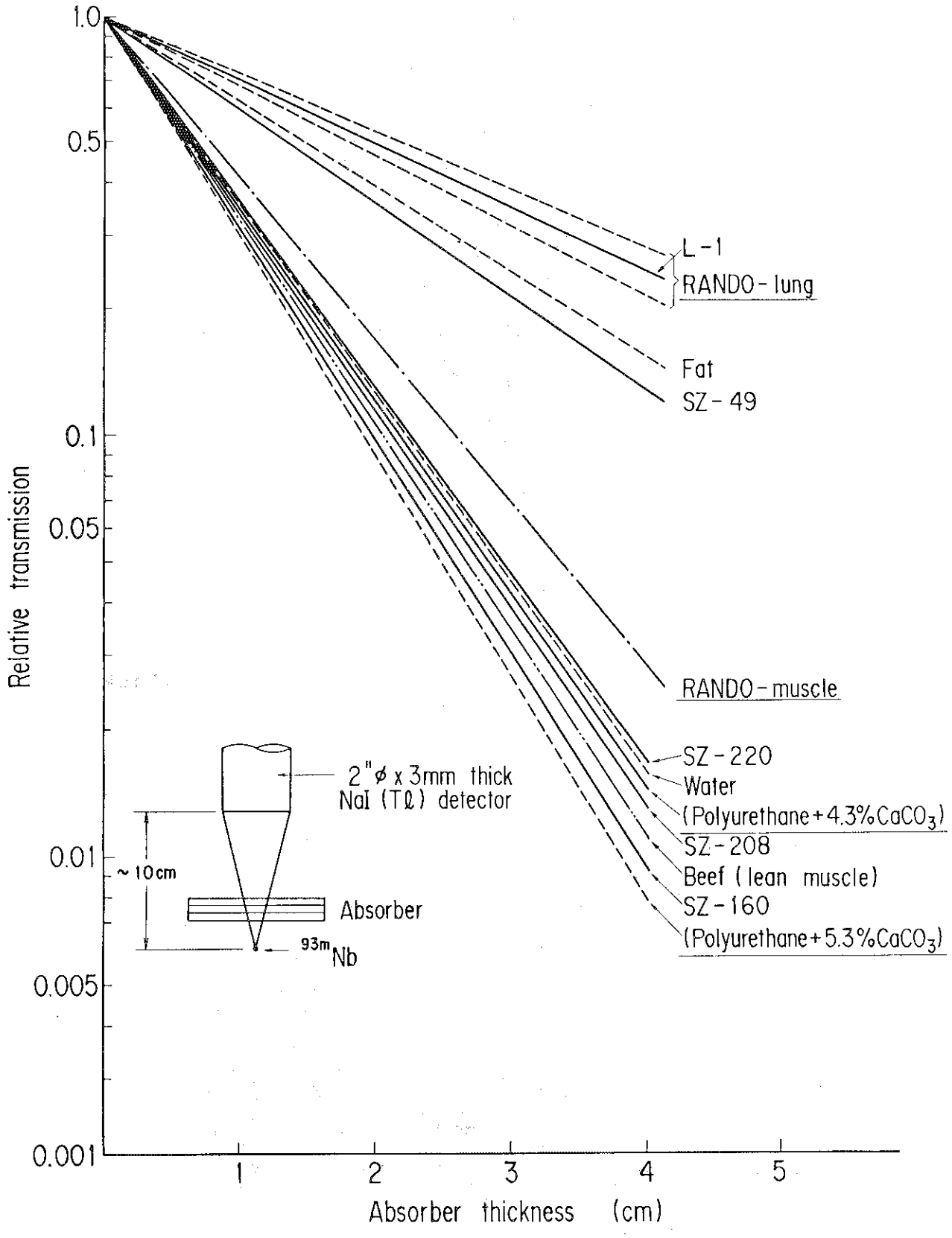

Fig.10 Relative X-ray transmission through beef, fat and others, obtained with detector without collimator (Data of polyurethane added $CaCO_3$ were quoted from Griffith's paper[2], for comparison.)

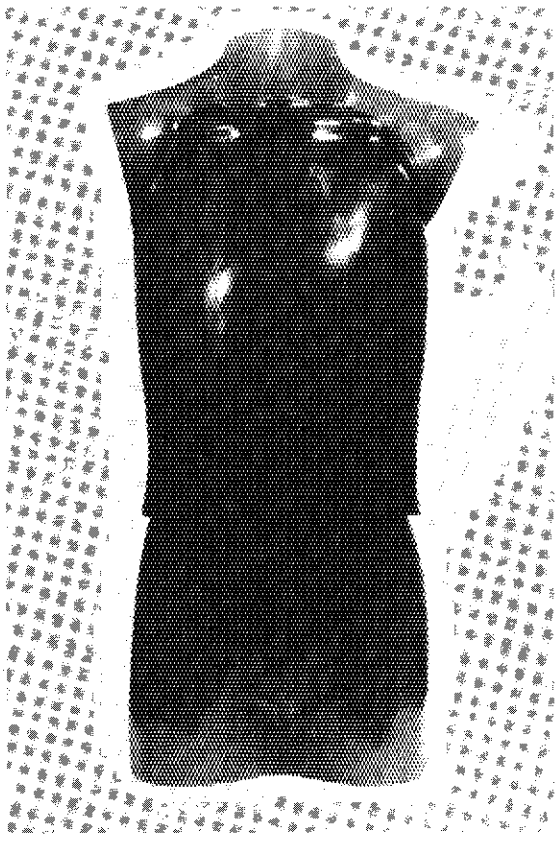

Fig. 11(a) Completed chest phantom with 0.8cm thick chest plate in place

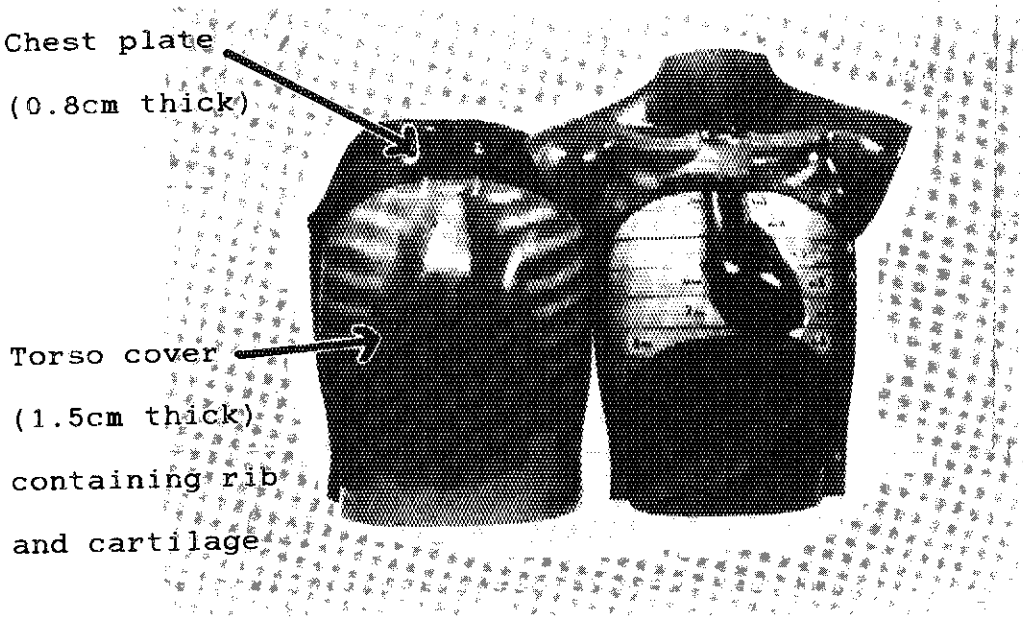

Fig. 11(b) Front view of chest phantom with chest plate and torso cover removed showing organs

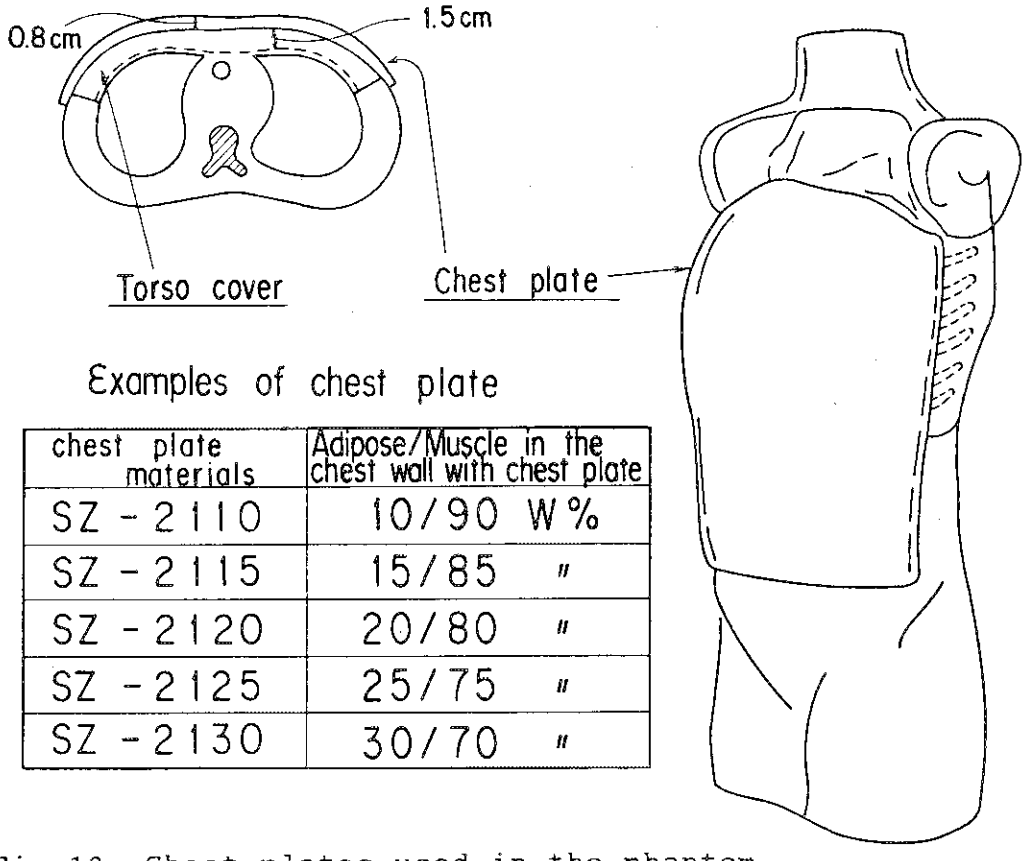

Examples of chest plate

chest plate materials	Adipose/Muscle in the chest wall with chest plate
SZ－2110	10/90 W%
SZ－2115	15/85 〃
SZ－2120	20/80 〃
SZ－2125	25/75 〃
SZ－2130	30/70 〃

Fig.12 Chest plates used in the phantom

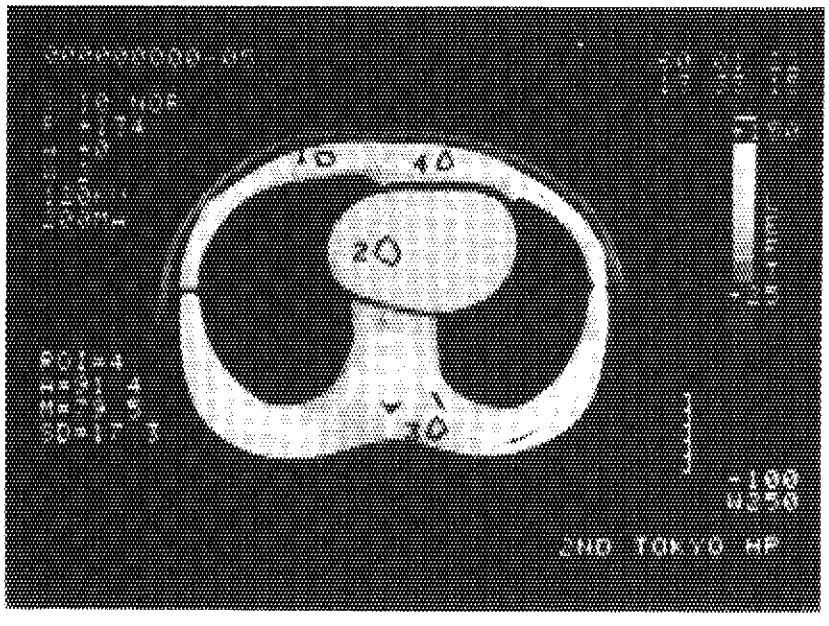

Fig. 13 A tomogram of lung region obtained with X-ray CT-scanner

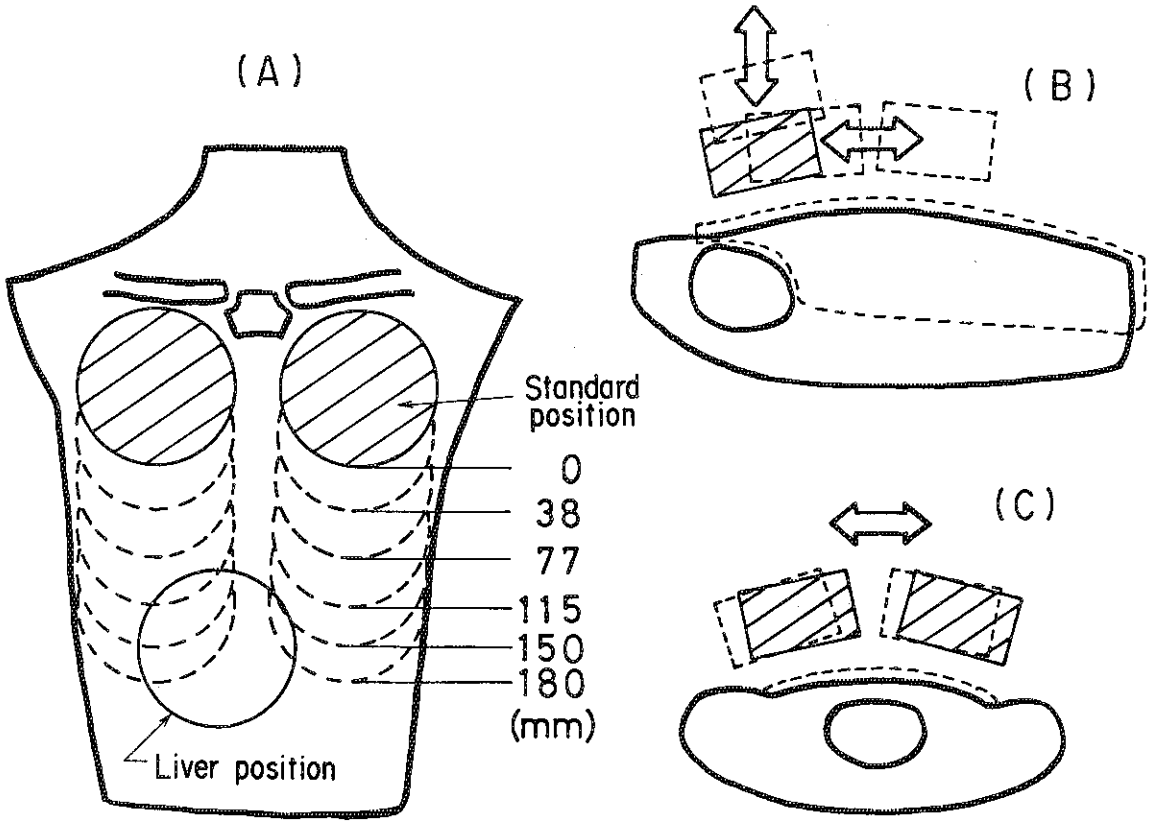

Fig.14 Detector to body geometry

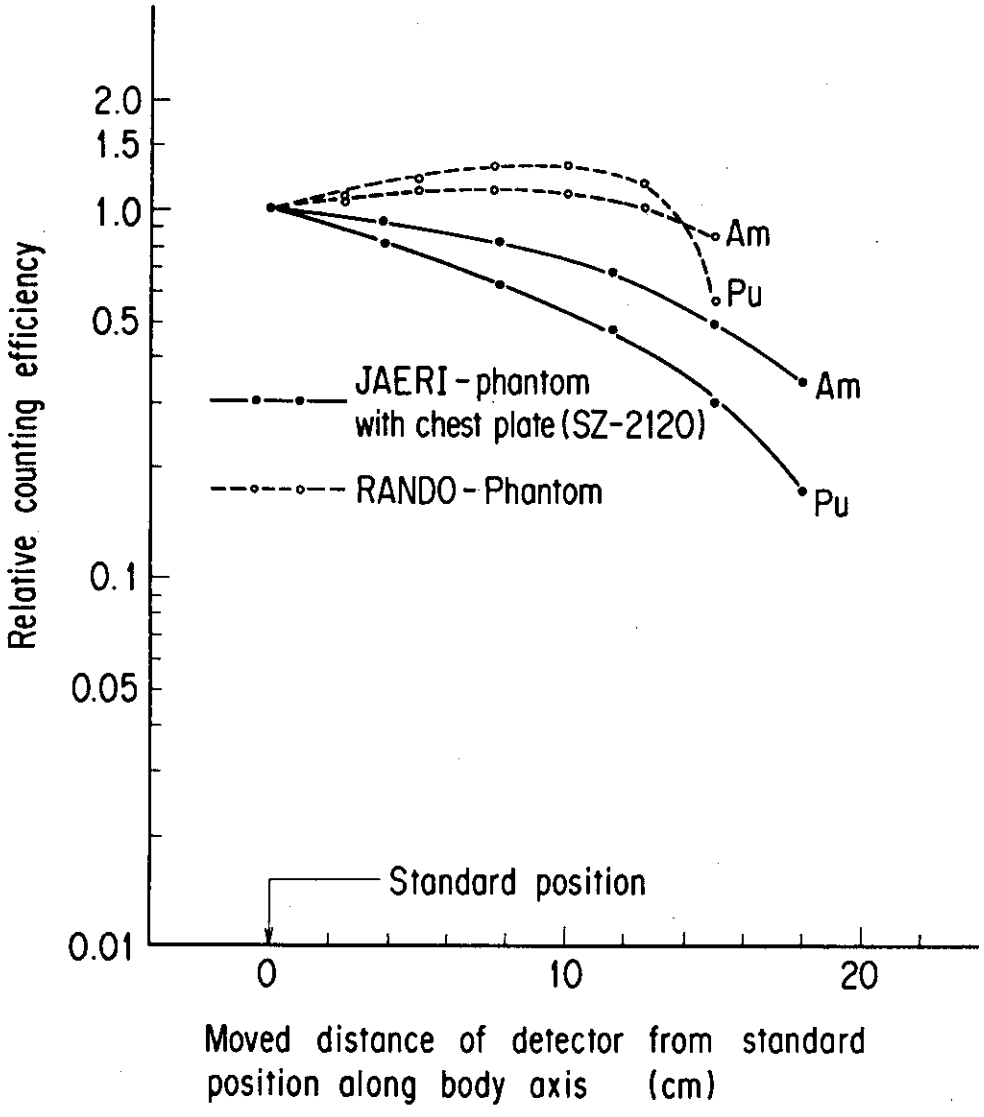

Fig.15 Variation of counting efficiency of detector moved from standard position to abdomen along the body axis

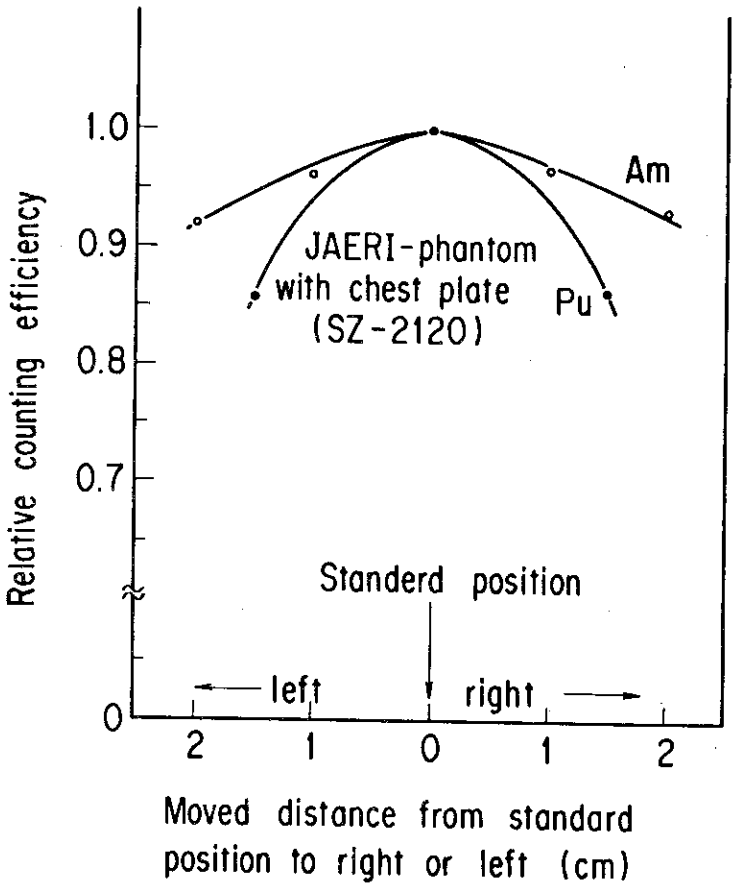

Fig.16 Variation of relative counting efficiency of detector moved to right and left at standard position

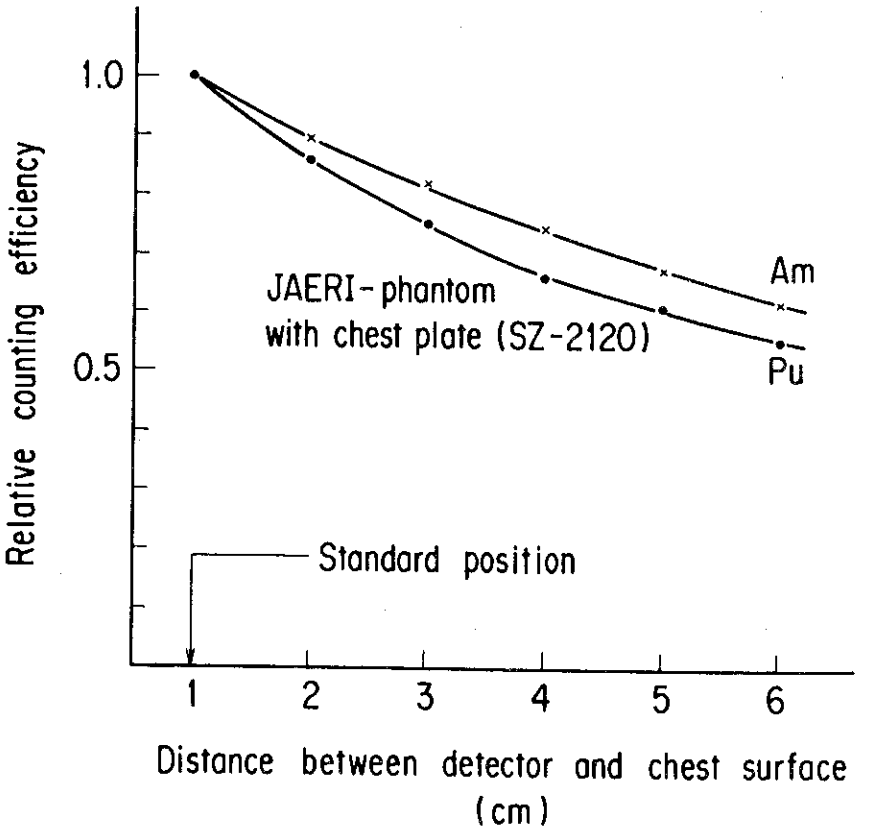

Fig.17 Decrease in counting efficiency of detector moved along external normal direction from chest at the standard position

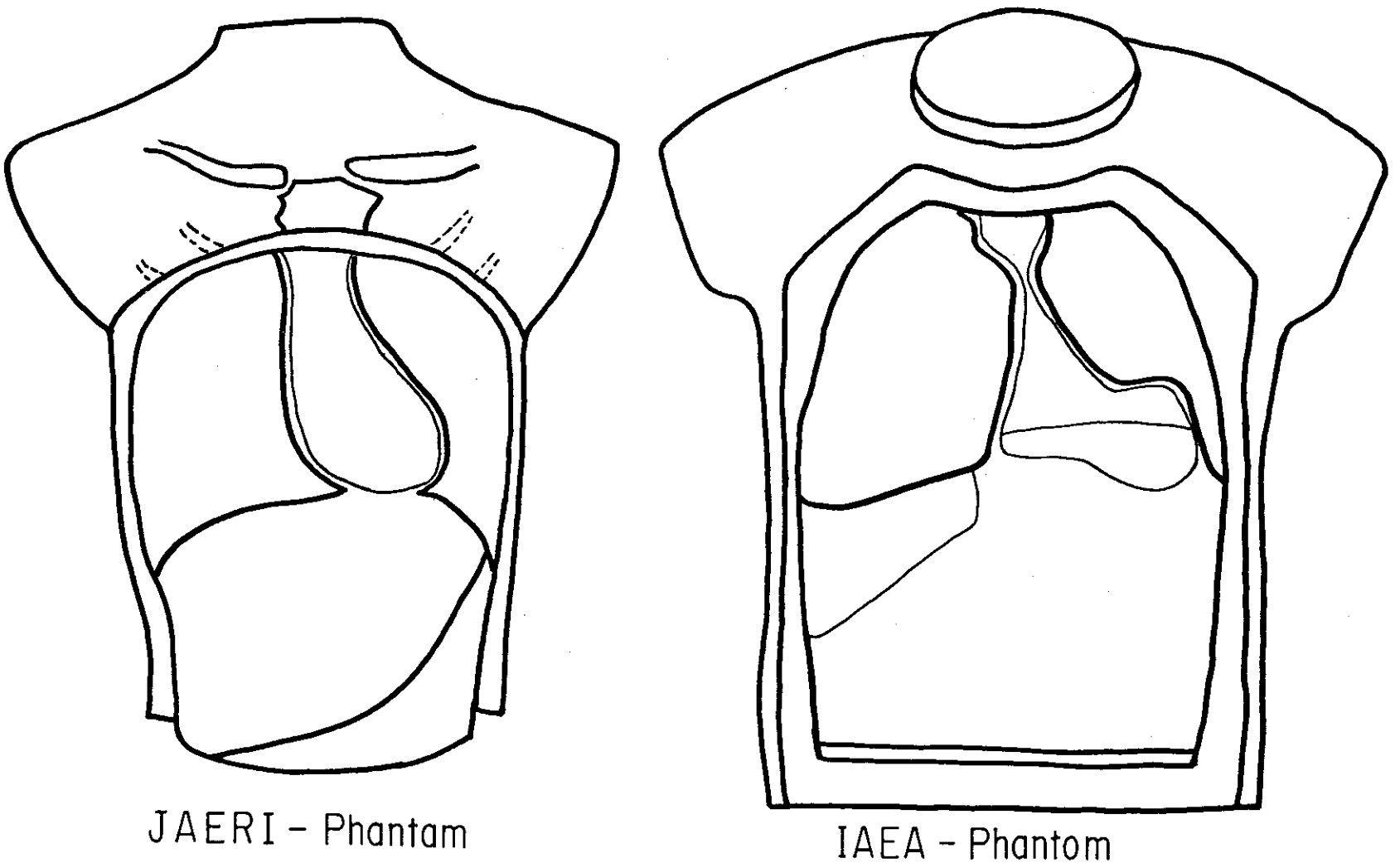

Fig.A-1 Illustration of front views of JAERI- and IAEA-phantoms without torso cover and chest plate

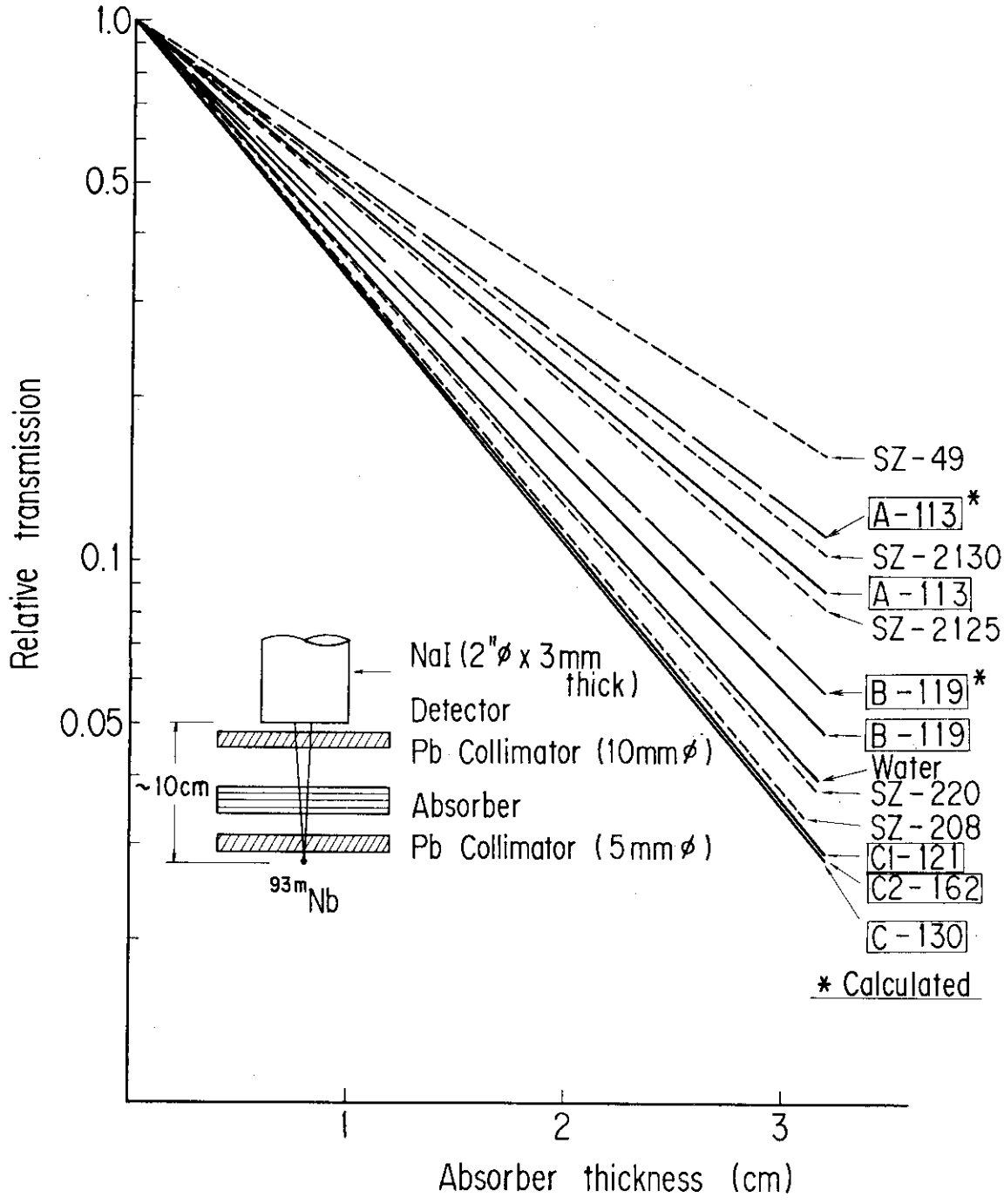

Fig.A-2 Comparison of X-ray transmission curves of IAEA-phantom materials with those of SZ-series materials (IAEA-phantom materials are A-113, B-119, C-130 and C2-162.)

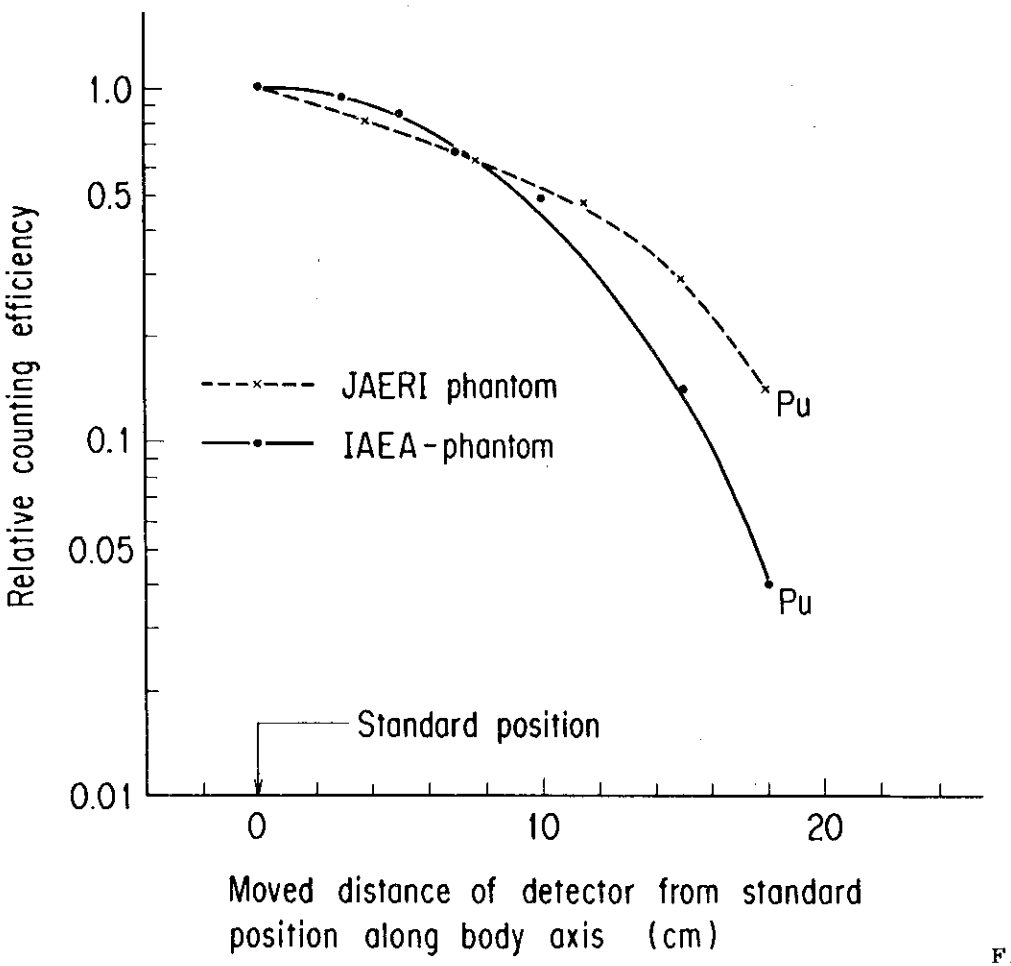

Fig.A-3 Comparison of relative variation of body-axis counting efficiency in IAEA-phantom with that in JAERI-phantom

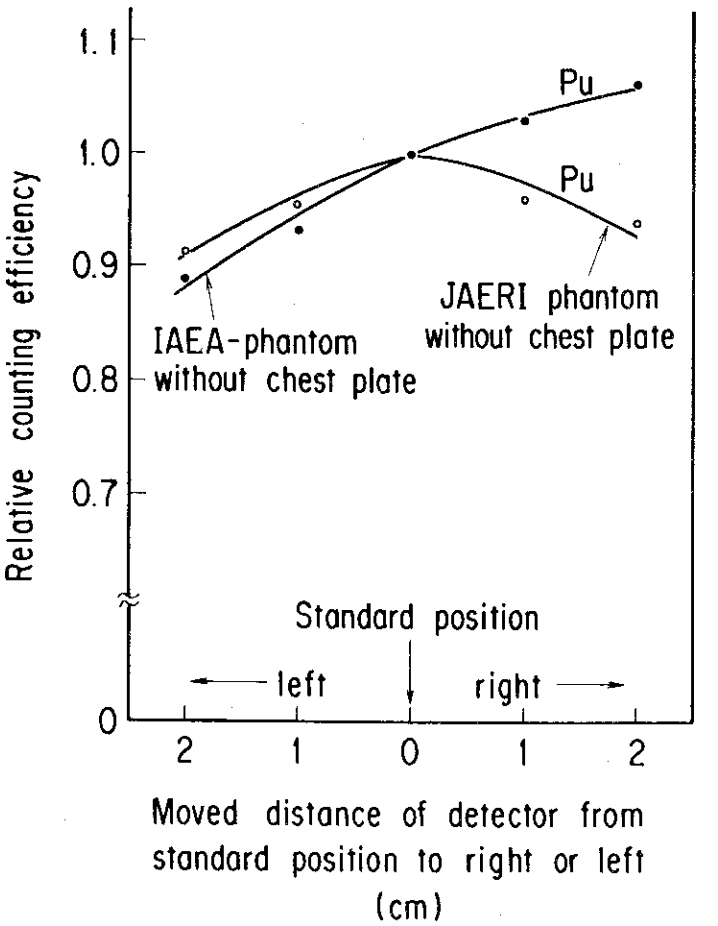

Fig.A-4 Comparison of relative variation of counting efficiency of detector moved right and left at standard position in IAEA-phantom with that in JAERI-phantom